Large Eddy Simulation of a Turbulent Flow in a T-Junction

Jungwoo Kim and Jae Jun Jeong

Thermal Hydraulics Safety Research Division
Korea Atomic Energy Research Institute
1045 Daedeok-daero, Yuseong-gu, Daejeon, 305-353, Republic of Korea
Tel.:+82-42-868-2136, Fax:+82-42-868-4801, Email: kimjw@kaeri.re.kr

1. Introduction

The problem of thermal fatigue is frequently encountered in the pipes where two flows with different temperatures mix together. The T-junction is one of the typical components with a considerable potential of thermal fatigue (Chapuliot et al. 2005; Hu & Kazimi 2006; Lee et al. 2009) and is used in many thermohydraulic systems such as combustion engines, turbines, exhaust systems, reheat systems and so on. The T-junction configuration consists of two pipe systems intersected perpendicularly, and they are called main and branch pipes. In nuclear thermo-hydraulic society, this T-junction configuration has received much interest because the two freestreams with a higher and lower temperatures mix and then induce thermal fatigue generated by the temperature change in the wall, which is known as the main source of the structural damage of T-junction. However, the issues related to this problem remain unresolved because the flow in the T-junction is a completely three-dimensional turbulent flow in that the interaction between the main and the branch flows creates the complex turbulent structure including the wide distribution types of eddies.

In the present study, a numerical simulation is performed to investigate the phenomenon related to the turbulent flow and heat transfer in a T-junction. It is well known from literature that the problem cannot be accurately predicted by RANS- or URANS-based simulation approaches (Peniguel 1998). This results from the well-known overestimation of κ at stagnation points. The advected overestimation of ν_t eventually leads to a severe damping of the flow structure downstream. The difficulty in obtaining proper swirling flows in the T-junction with a $\kappa-\varepsilon$ model is likely to be partly explained by such a behavior. In that respect, large eddy simulation (LES) can be a good approach because it is regarded as an intermediate technique between the direct numerical simulation (DNS) and Reynolds average approaches. In LES, large, energy-carrying structures are directly calculated in grid space while the smaller scales are modeled with a subgrid-scale model. As a similar example, in terms of a jet in crossflow similar to T-junction, it has been reported that RANS calculations provide a reasonably good prediction of mean velocities and a poor prediction of turbulence intensities (Muppidi & Mahesh 2007). On the other hand, some recent LES simulation results have shown that they can reasonably predict mean velocities as well as turbulence intensities (Yuan et al. 1999; Schluter & Schonfeld 2000).

Therefore, in order to get better understanding of this phenomenon, the flow in the T-junction will be investigated by using the large eddy simulation technique which is newly regarded as a good turbulence simulation tool.

2. Problem Descriptions

In this section, the T-junction configuration will be described in detail. In the present study, the configuration is taken from the experiment performed at Vattenfall Research and Development Laboratory at Alvkarlevy, Sweden. The details of the T-junction configuration considered in that study are given as shown in figure 2.

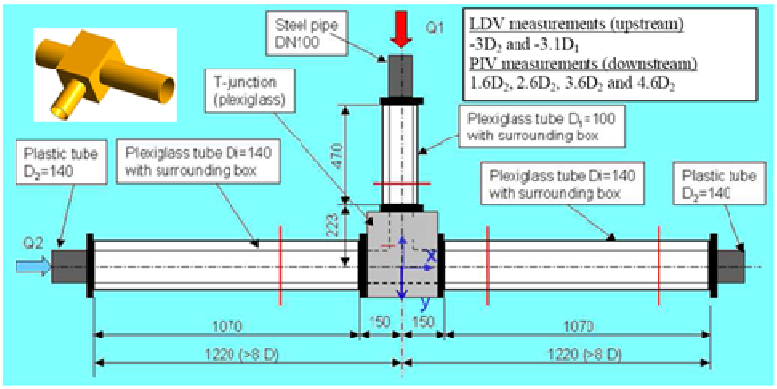

Figure 1. T-junction configuration considered in the experiment performed at Vattenfall Research and Development Laboratory at Alvkarlevy, Sweden.

As for the flow parameters, the volumetric flow rates in the main and branch pipes are 9 Liter/sec and 6 Liter/sec, respectively. Water is used as working fluid. As a result, the Reynolds number considered here is based on the diameter and bulk velocity of the pipe and so Re's are 81,000 and 76,000, respectively, for the main and branch pipes. The temperatures for the cold (main pipe) and hot (branch pipe) inlets are 19^{o}C and 36^{o}C, respectively.

3. Numerical Details

The governing equations considered in this study are as below.

$$\frac{\partial \overline{u}_i}{\partial x_i} - q = 0, \tag{1}$$

$$\frac{\partial \overline{u}_i}{\partial t} + \frac{\partial \overline{u}_i \overline{u}_j}{\partial x_j} = -\frac{1}{\rho}\frac{\partial \overline{p}}{\partial x_i} + \nu \frac{\partial^2 \overline{u}_i}{\partial x_j \partial x_j} - \frac{\partial \tau_{ij}}{\partial x_j} + f_i, \tag{2}$$

$$\frac{\partial \overline{\theta}}{\partial t} + \frac{\partial \overline{\theta} \overline{u}_j}{\partial x_j} = \alpha \frac{\partial^2 \overline{\theta}}{\partial x_j \partial x_j} - \frac{\partial q}{\partial x_j} + h, \tag{3}$$

As shown in the equations, the temperature is treated as passive scalar in this study. According to Hirota et al. (2008), the velocity distributions measured under the isothermal condition agreed with those obtained with T_h=60^{o}C and T_c=12^{o}C, suggesting that the buoyancy effect on the mixing is negligibly small. In this study, the temperature difference is 17^{o}C so the present treatment of the temperature is reasonable.

Regarding SGS model, the Smagorinsky model had been much used in an earlier period of large eddy simulation. However, the Smagorinsky model is well known to have the drawback that the model coefficient should be predetermined as a constant in space and time although it should depend on the flow type, resolution and local flow information. To overcome this problem, the dynamic Smagorinsky model was recently developed, which has played a key role in making LES a popular tool for turbulence simulation. In DSM, the model coefficient is dynamically determined using the Germano identity based on the concept of the scale-invariance. DSM actually requires averaging over homogeneous direction and/or ad hoc clipping. This fact hinders the application of DSM to complex flows in which there is no homogeneous direction. A few methodologies have been proposed in the framework of DSM to overcome this problem. The representative ones are the dynamic localization model (Ghoshal et al. 1995) and the Lagrangian model (Meneveau 1996). However, additional efforts for the implementation of these models such as the iterative solution of the integral equation or interpolation for the pathline averaging are nontrivial overheads.

In that respect, in this paper the Vreman model was considered that is an eddy viscosity type SGS model of the form

$\left(\tau_{ij}-\frac{1}{3}\tau_{kk}\delta_{ij}=-2\nu_T\bar{S}_{ij}\right)$ because the model is quite robust and is readily applicable to complex turbulent flows where there is no homogeneous direction. The Vreman model has an advantage that for various laminar flows zero SGS dissipation is theoretically guaranteed in contrast with other eddy viscosity type SGS models such as Smagorinsky model. In the Vreman model, the eddy viscosity is defined as $\nu_T=C_v\sqrt{\frac{\Pi_\beta}{\bar{\alpha}_{ij}\bar{\alpha}_{ij}}}$ $\left(\bar{\alpha}_{ij}=\frac{\partial\bar{u}_j}{\partial x_i}\right.$, $\left.\Pi_\beta=\beta_{11}\beta_{22}-\beta_{12}^2+\beta_{11}\beta_{33}-\beta_{13}^2+\beta_{22}\beta_{33}-\beta_{23}^2\right.$, $\beta_{ij}=\sum_{m=1}^{3}\bar{\Delta}_m^2\bar{\alpha}_{mi}\bar{\alpha}_{mj}$, where C_v is the model coefficient).

In this paper, C_v is determined through a dynamic procedure based on the global equilibrium between the SGS dissipation and the viscous dissipation (Park et al. 2006).

$$C_v=\frac{\nu(\gamma-1)<\bar{\alpha}_{ik}\bar{\alpha}_{ik}>_V}{2<\sqrt{\frac{\Pi_\beta}{\bar{\alpha}_{jl}\bar{\alpha}_{jl}}}\bar{S}_{ik}\bar{S}_{ik}>_V}. \tag{4}$$

Here, V is the volume of the entire computational domain. $\gamma=\frac{<\overline{\alpha_{ik}\alpha_{ik}}>_V}{<\bar{\alpha}_{ik}\bar{\alpha}_{ik}>_V}$

$$\gamma=\frac{<\overline{\alpha_{ik}\alpha_{ik}}>_V}{<\bar{\alpha}_{ik}\bar{\alpha}_{ik}>_V}=\frac{<\hat{\alpha}_{ik}\hat{\alpha}_{ik}>_V<\bar{\alpha}_{ik}\bar{\alpha}_{ik}>_V^2}{<\tilde{\bar{\alpha}}_{ik}\tilde{\bar{\alpha}}_{ik}>_V^3}. \tag{5}$$

Here, $\tilde{\bar{\alpha}}_{ij}$ is the test filtered quantity with the filter size of $\tilde{\Delta}=2\bar{\Delta}$ and $\hat{\alpha}_{ij}$ is the second test filtered quantity with $\hat{\Delta}=4\bar{\Delta}$. Please note that the accuracy of subgrid-scale model used in the present study has been confirmed by *a priori* and *a posteriori* tests for various turbulence flows (forced isotropic turbulence, turbulent channel flow, flows over a circular cylinder and a sphere; Park *et al*. 2006).

Also in order to efficiently simulate the flow in the T-junction, the immersed boundary (IB) method developed by Kim et al. (2001) and Kim & Choi (2004) is used. Figure 2 shows the schematic diagram of the IB method. As shown in this figure, in IB method, a body in the flow field is considered as a kind of momentum forcing in the Navier-Stokes equations rather than a real body. It is known to have good advantages in mesh generation and computational time efficiency as compared to the unstructured grid approach because the IB method can handle complex geometry in framework of Cartesian grid. This method has been successfully applied to the various flows (Yun et al. 2004; Park et al. 2006) The method of determining f_i, q and h is fully described in Kim et al. (2001) and Kim & Choi (2004).

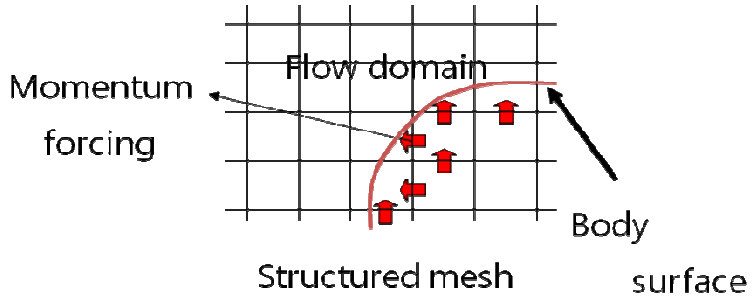

Figure 2. Schematic diagram of the immersed boundary (IB) method.

The basic computational details for this study are as follows. The time integration scheme considered in this study is based on the fractional step method (Kim & Moin, 1985), and is composed of the second-order accurate Crank-Nicolson method for the diffusion terms in the momentum and

energy equations and third-order accurate Runge-Kutta method for the convection terms in their equations. Also, the second-order accurate central scheme is considered as the spatial difference scheme because it is known as being free from dissipation error which plays a crucial role in determining the performance of the SGS model.

$$\frac{\hat{u}_i^k - u_i^{k-1}}{\Delta t} = \frac{\alpha_k}{\mathrm{Re}} L(\hat{u}_i^k) + \frac{\alpha_k}{\mathrm{Re}} L(u_i^{k-1}) - 2\alpha_k \frac{\partial p^{k-1}}{\partial x_i} - \gamma_k N(u_i^{k-1}) - \rho_k N(u_i^{k-2}) + f_i^k, \quad (6)$$

$$\frac{\partial^2 \phi^k}{\partial x_i \partial x_i} = \frac{1}{2\alpha_k \Delta t}\left(\frac{\partial \hat{u}_i^k}{\partial x_i} - q^k\right), \quad (7)$$

$$u_i^k = \hat{u}_i^k - 2\alpha_k \Delta t \frac{\partial \phi^k}{\partial x_i}, \quad (8)$$

$$p^k = p^{k-1} + \phi^k - \frac{\alpha_k \Delta t}{\mathrm{Re}} \frac{\partial^2 \phi^k}{\partial x_j \partial x_j}, \quad (9)$$

$$\frac{\theta^k - \theta^{k-1}}{\Delta t} = \frac{\alpha_k}{\mathrm{Re}\,\mathrm{Pr}} L(\theta^k) + \frac{\alpha_k}{\mathrm{Re}\,\mathrm{Pr}} L(\theta^{k-1}) - \gamma_k N(\theta^{k-1}) - \rho_k N(\theta^{k-2}) + h^k, \quad (10)$$

where $L() = \partial^2() / \partial x_j \partial x_j$, $N() = \partial u_j() / \partial x_j$, $\hat{u}_i$ is the intermediate velocity, ϕ is the pseudo-pressure, Δt and k are the computational time step and substep's index, respectively. α_k, γ_k, ρ_k are the coefficients of RK3. Here, as shown in figure 1, f_i, q and h are defined inside the immersed body or on the cell containing the immersed boundary, and zero elsewhere. The grid points for the momentum forcing are located in a staggered fashion like the velocity components defined on a staggered grid. Also, the grid points for the mass and heat source/sink are located at the cell centers like the pressure and temperature.

Figure 3 shows the computational domain and grid systems used in the present study. The number of the total grid points used in this study is approximately 7 million. And the fluid region consists of approximately 4 million grid points. Based on previous studies on the jet in crossflow (Yang 2000; Muppidi & Mahesh 2007; Denev et al. 2009), the present grid resolution is likely to be marginal. More detailed information on grid systems is as below:

1) Number of cells

Main pipe: $640\,(N_x) \times 240\,(N_y) \times 24\,(N_z) = 3{,}686{,}400$.

Branch pipe: $240\,(N_x) \times 100\,(N_y) \times 24\,(N_z) = 576{,}000$.

2) Minimum cell length

Main pipe: $\Delta x_{\min} / D_b = 0.004$, $\Delta y_{\min} / D_b = 0.005$, $\Delta z_{\min} / D_b = 0.06$.

Branch pipe: $\Delta x_{\min} / D_b = 0.004$, $\Delta y_{\min} / D_b = 0.005$, $\Delta z_{\min} / D_b = 0.06$.

3) Maximum cell length

Main pipe: $\Delta x_{\max} / D_b = 0.155$, $\Delta y_{\max} / D_b = 0.063$, $\Delta z_{\max} / D_b = 0.06$.

Branch pipe: $\Delta x_{\max} / D_b = 0.0425$, $\Delta y_{\max} / D_b = 0.155$, $\Delta z_{\max} / D_b = 0.06$.

Also, in terms of the velocity boundary condition, the inlet boundary conditions for main and branch pipes are Dirichlet type and the convective boundary condition is taken as the outlet boundary condition. On the other hand, in terms of the temperature boundary condition, the constant heat flux condition is given at all the regions except the inlets and outlet as shown in figure 3(a).

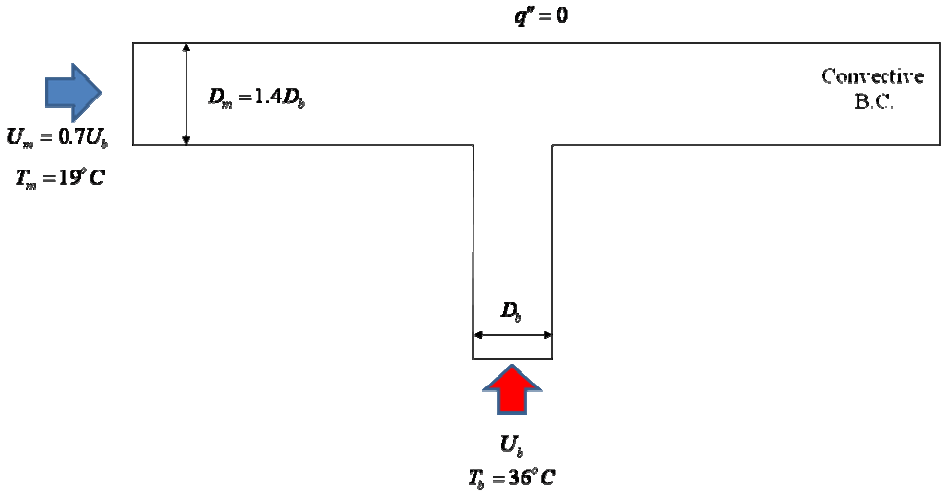

(a)

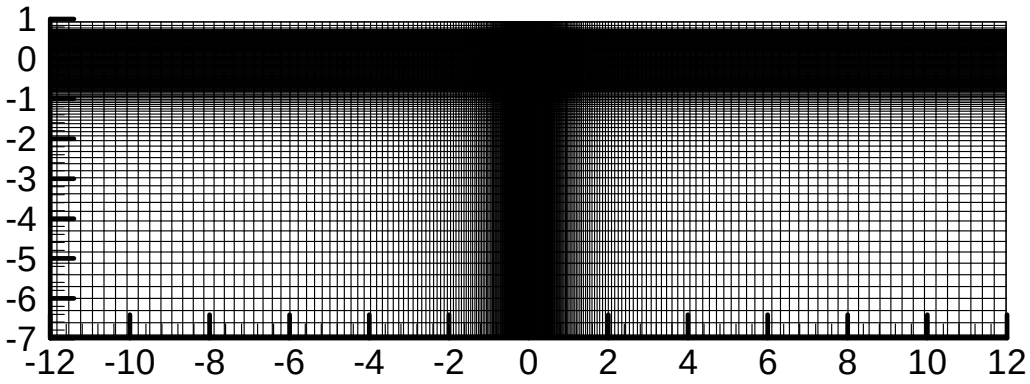

(b)

Figure 3. (a) Computational domain and (b) grid system.

4. Numerical Results

Figure 4 shows the instantaneous spanwise Vorticity (z-component Vorticity). The coordinate adopted in this study is shown in figure 1. In this figure it is observed to be strongly interacted the vortical structures shed from the intersectional region between the main and branch pipes and those coming upstream along the main pipe. As a result, complicated three-dimensional vortical structures exist in the T-junction. They are seen as the main source of a pipe damage problem occurring in this T-junction configuration (Hosseini et al. 2009).

According to Hu & Kazimi (2006), the flow type considered in this study can be classified into three kinds depending on the momentum ratio of the entering flows, $M_R = \dfrac{\rho_m V_m^2 D_m \times D_b}{\rho_b V_b^2 \pi (D_b/2)^2}$ where M_R is the momentum ratio. The three flow patterns are as follows:

Wall jet $M_R > 1.35$,

Deflecting jet $0.35 < M_R < 1.35$,

Impinging jet $M_R < 0.35$.

In this study, $M_R = \dfrac{\rho_m V_m^2 D_m \times D_b}{\rho_b V_b^2 \pi (D_b/2)^2} = 1.04$. The present numerical result is consistent with the above classification in that the flow pattern formed looks like the deflecting jet as shown in figure 1.

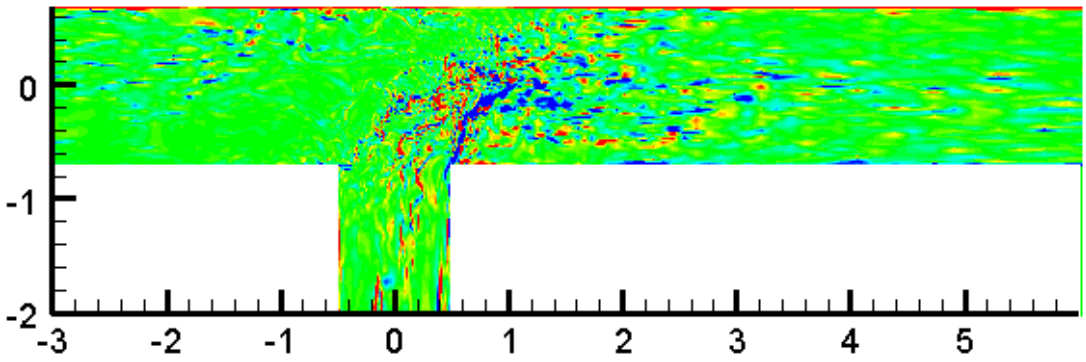

Figure 4. Instantaneous spanwise vorticity contours.

To see the difference between SGS models, figure 5 shows the instantaneous spanwise vorticity contour drawn from the numerical result obtained by using Vreman model. As shown in figure 5, the small vortical structures are not well captured in the case of Vreman model as compared to the Dynamic Vreman model shown in figure 4.

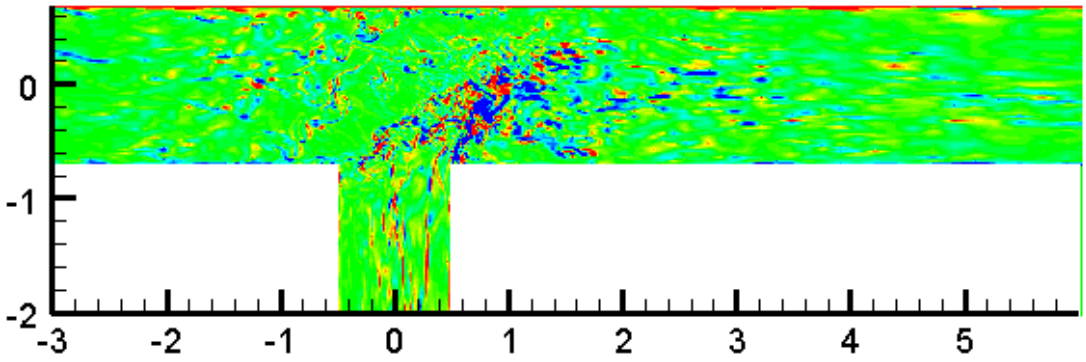

Figure 5. Instantaneous spanwise vorticity contours calculated by Vreman model.

Figures 6-8 show the time-averaged x, y, z-component velocity distributions in z=0 and y=0. As shown in figure 6, the x-component velocity shows negative values near the bottom wall at x/D_b=1.6, which results from the existence of the separation region observed in figure 4. Here, subscript 'b' means the branch pipe. The present duration time taken for averaging (~$12D_b/U_b$) cannot be said to be sufficiently long, but be not insufficient to see the turbulent field in an averaged sense because the dominant frequency ($St=fU_b/D_b$) is around 0.5 (as shown in figure 12 later), which indicates that the dominant vortical structures have the period of around $2D_b/U_b$. Also, the averaged data with respect to the time duration are found to be varied with the error of almost 5% in terms of the streamwise components and more or less 20% in terms of the two other components if assessed to the time duration of $12D_b/U_b$ and $6D_b/U_b$. As x/D_b increases, the velocity recovers to be positive. Also, y-component velocity has a small value in most region, whereas z-component velocity has a little bigger value near the bottom wall at z=0, which is comparable to x-component velocity.

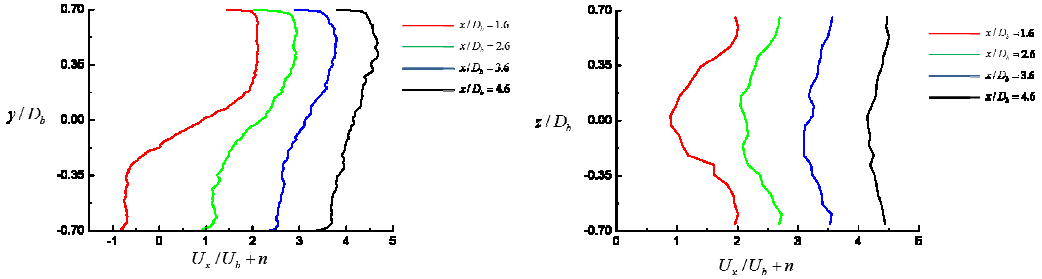

(a) (b)

Figure 6. Time-averaged x-component velocity distribution: (a) z=0; (b) y=0.

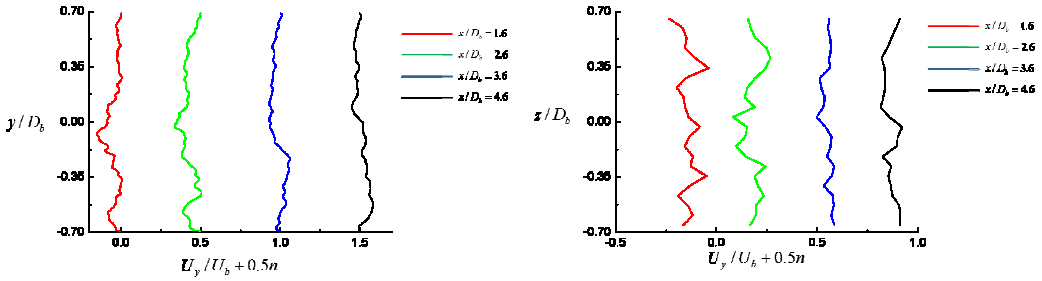

(a) (b)

Figure 7. Time-averaged y-component velocity profiles: (a) z=0; (b) y=0.

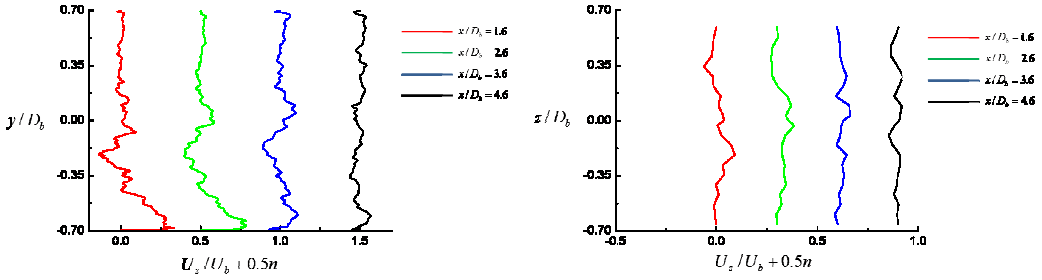

(a) (b)

Figure 8. Time-averaged z-component velocity profiles: (a) z=0; (b) y=0.

Figures 9-11 show the time-averaged x, y, z-component velocity distributions in z=0 and y=0. As shown in these figures, the velocity fluctuations show maximum values in the center region. However, in terms of rms x-component velocity fluctuations, in the top wall region at larger x/D_b, they become comparable to that in the center of the pipe as shown in figure 9(a). On the other hand, rms z-component velocity fluctuations have a relatively large value in the bottom wall region as compared to those in the top wall region.

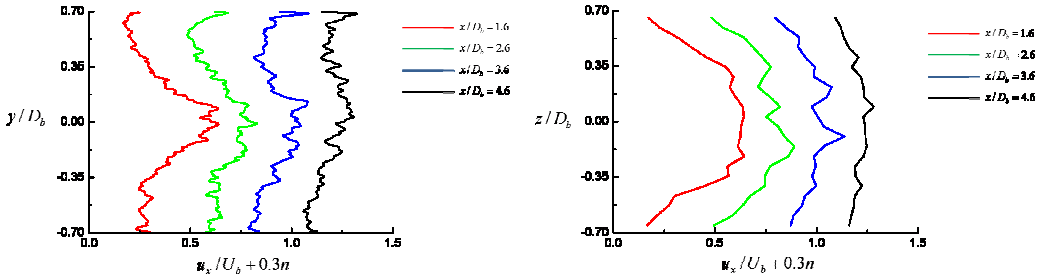

(a) (b)

Figure 9. Rms x-component velocity fluctuation profiles: (a) z=0; (b) y=0.

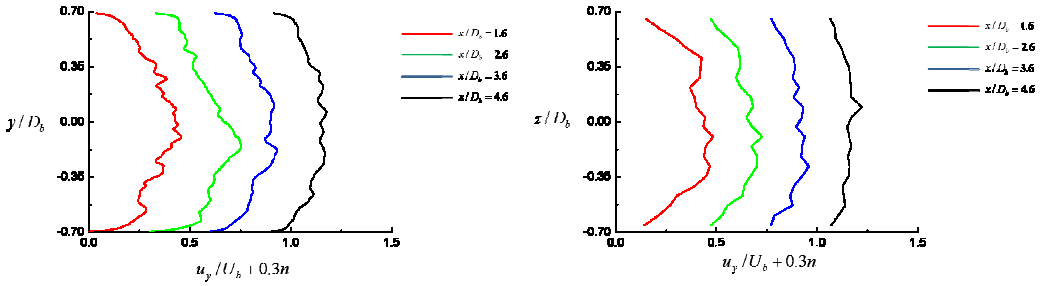

(a) (b)

Figure 10. Rms y-component velocity fluctuation profiles: (a) z=0; (b) y=0.

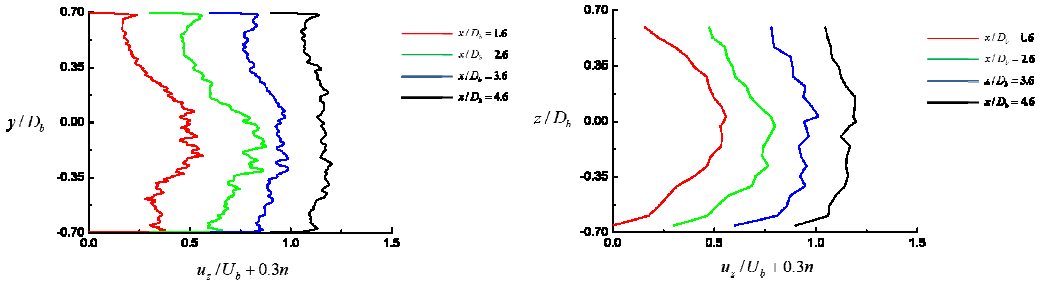

(a) (b)

Figure 11. Rms z-component velocity fluctuation profiles: (a) z=0; (b) y=0.

The fatigue cracking of the pipe wall resulting from the cyclical thermal stress is caused by the coolant fluctuations. Therefore, the frequency of the coolant oscillation, together with the coolant fluctuation magnitude, has been considered to be important to evaluate the thermal fatigue. In order to see the dominant frequency in the present study, the power spectra of the x-component velocity at several x-locations are shown in figure 12. As shown in this figure, although the dominant frequencies become different depending on the azimuthal angle, it almost has the value of St~0.5. According to previous literature, an oscillation observed in T-junction is reported to have a frequency in the order of several HZ (Wakamatsu et al. 1995), which corresponds to the nondimensional frequency, Strouhal number with an order of O(0.1).

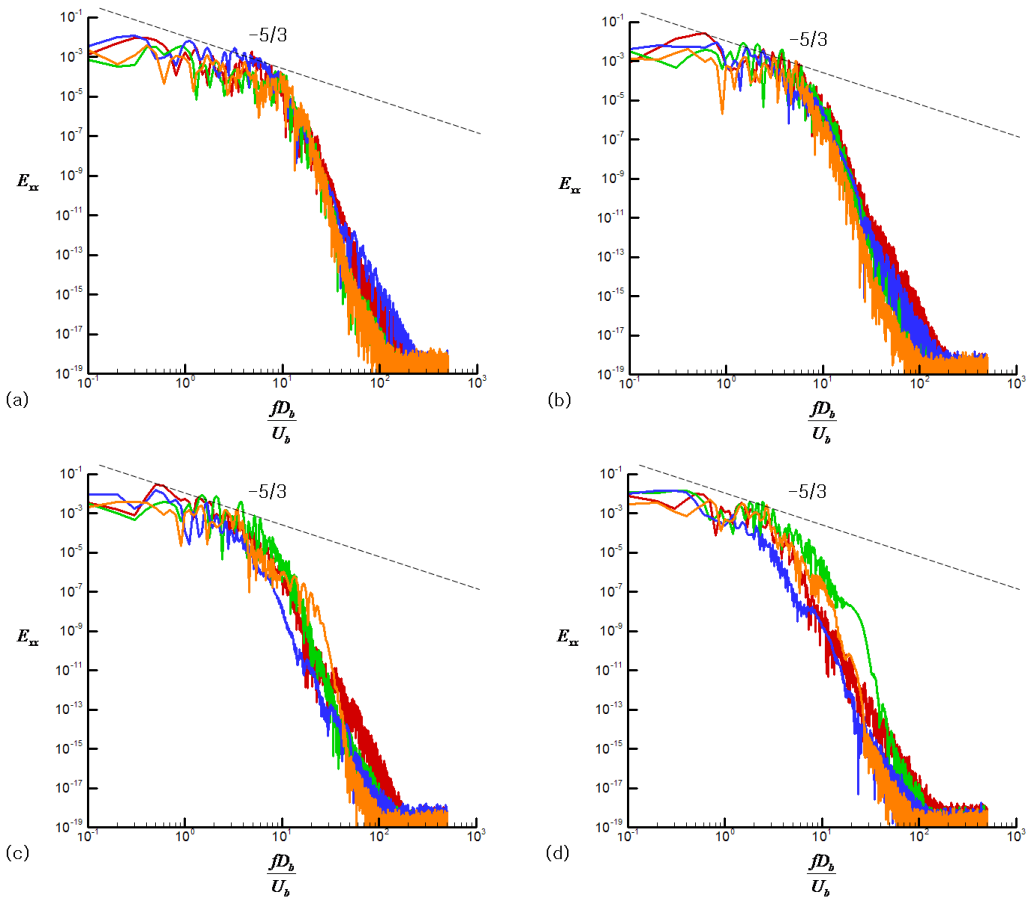

Figure 12. Power spectra of the x-component velocity at some axial locations: (a) x/D_b=1.6; (b) x/D_b=2.6; (c) x/D_b=3.6; (d) x/D_b=4.6. Red: y/D_b=0.69, z/D_b=0; green: y/D_b=0, z/D_b=-0.69; blue: y/D_b=-0.69, z/D_b=0; orange: y/D_b=0, z/D_b=0.69. Dashed line denotes the slope corresponding to the Kolmogorov subrange.

5. Summary

In the present study, a large eddy simulation was performed in order to further understand the thermal fatigue in a T-junction. Based on the numerical results from the LES, the velocity fluctuations and the frequency were examined because they have been regarded as being of primary importance in the study on the thermal fatigue according to previous studies. In the final presentation, the study on the statistics related to the temperature field will be presented. Also, if possible to have an access to the experimental data, the final presentation would include the comparison of the present simulation to the Vattenfall experiment.

Acknowledgement

This work was supported by Nuclear Research & Development Program of Nuclear Research and Development Program of the NRF (National Research Foundation of Korea) grant funded by the MEST (Ministry of Education, Science and Technology) of the Korean government (Grant code: M20702040002-08M0204-00210).

References

C. Bruecker, 1997, Study of the three-dimensional flow in a T-junction using a dual-scanning method for three-dimensional Scanning-Particle Image Velocimetry (3D SPIV), Exp. Therm. Fluid Sci., 14, 35.

S. Chapuliot, C. Gourdin, T. Payen, J. P. Magnaud and A. Monavon, 2005, Hydro-thermal-mechanical

analysis of thermal fatigue in a mixing tee, Nucl. Eng. Des., 235, 575.
G. Chochua, W. Shyy, S. Thakur, A. Brankovic, K. Lienau, L. Porter and D. Lischinksy, 2000, A computational and experimental investigation of turbulent jet and crossflow interaction, Numer. Heat Transfer, Part A., 38, 557.
M. Germano, U. Piomelli, P. Moin and W. Cabot, 1991, A dynamic subgrid-scale eddy viscosity model, Phys. Fluids A 3, 1760.
S. Ghosal, T. S. Lund, P. Moin and K. Akselvoll, 1995, A dynamic localization model for large eddy simulation of turbulent flows, J. Fluid Mech., 286, 229.
M. Hirota, M. Kuroki, H. Nakayama, H. Asano and S. Hirayama, 2008, Promotion of turbulent thermal mixing of hot and cold airflows in T-junction, Flow Turbulence Combust, 81, 321.
S. M. Hosseini, H. Yuki and H. Hashizume, 2008, Classifications of turbulent jets in a T-junction area with a 90-degree bend upstream, Int. J. Heat Mass Transfer, 51, 2444.
S. M. Hosseini, K. Yuki and H. Hashizume, 2009, Experimental investigation of flow field structure in mixing tee, J. Fluids Eng., 131, 051103.
L.-W. Hu and M. S. Kazimi, 2006, LES benchmark study of high cycle temperature fluctuationscaused by thermal striping in a mixing tee, Int. J. Heat Fluid Flow, 27, 54.
M. Igarashi, N. Kimura, N. Tanaka and M. Kamide, 2003, LES analysis of fluid temperature fluctuations in a mixing tee pipe with the same diameters, Proc. 11th Int. Conf. On. Nuclear Engineering ICONE-11, Tokyo, Japan, April 20-23.
J. Kim, D. Kim and H. Choi, 2001, An immersed-boundary finite-volume method for simulations of flow in complex geometries, J. Comput. Phys., 171, 132.
J. Kim and H. Choi, 2004, An immersed-boundary finite-volume method for simulation of heat transfer in complex geometries, KSME Int. J., 18, 1026.
J. I. Lee, L.-W. Hu, P. Saha and M .S. Kazimi, 2009, Numerical analysis of thermal striping induced high cycle thermal fatigue in a mixing tee, Nucl. Eng. Des., 239, 833.
C. Meneveau, T. S. Lund and W. H. Cabot, 1996, A Lagrangian dynamic subgrid-scale model of turbulence, J. Fluid Mech., 319, 353.
K. J. Metzner and U. Wilke, 2005, European THERFAT project – Thermal fatigue evaluation of piping system Tee connections, Nucl. Eng. Des., 235, 473.
S. Muppidi and K. Mahesh, 2006, Passive scalar mixing in jets in crossflow, 44th AIAA Aerospace Science Meeting and Exhibit, Jan. 9-12. Reno, Neveda.
S. Muppidi and K. Mahesh, 2007, Direct numerical simulation of round turbulent jets in crossflow, J. Fluid Mech., 574, 59.
N. Park, S. Lee, J. Lee and H. Choi, 2006, A dynamic subgrid-scale eddy viscosity model with a global model coefficient, Phys. Fluids, 18, 125109.
C. Peniguel, 1998, Heat transfer simulation for industrial applications: needs, limitations, expectations, Int. J. Heat Fluid Flow, 19, 102-114.
J. Smagorinsky, 1963, General circulation experiments with the primitive equations, Mon. Weather Rev. 91, 99.
J. U. Schluter and T. Schonfeld, 2000, LES of jets in cross flow and its application to a gas turbine burner, Flow Turb. Combust., 65, 177.
A. W. Vreman, 2004, An eddy-viscosity subgrid-scale model for turbulent shear flow: Algebraic theory and application, Phys. Fluids, 16, 3670.
M. Wakamatsu, H. Nei and K. Hashiguchi, 1995, Attenuation of temperature fluctuation in thermal striping, J. Nucl. Sci. Tech., 32, 752.
Z. Yang, 2000, Large eddy simulation of fully developed turbulent flow in a rotating flow, Int. J. Numer. Meth. Fluids, 33, 681.
K. Yuki, Y. Sugawara and S. M. Hosseini, 2008, Influence of secondary flow generated in a 90-degree bend on the thermal-hydraulic characteristics in a mixing tee, Nucl. Sci. Eng., 158, 194.
G. Yun, D. Kim and H. Choi, 2006, Vortical structures behind a sphere at subcritical Reynolds numbers, Phys. Fluids 18, 015102.
L. L. Yuan, R. L. Street and J. H. Ferziger, 1999, Large eddy simulations of a round jet in crossflow, J. Fluid Mech., 379, 71.